Comments on tails in Schwarzschild spacetimes.

Janusz Karkowski*, Zdobysław Świerczyński+ and Edward Malec*
* *Institute of Physics, Jagiellonian University, 30-059 Cracow, Reymonta 4, Poland.*
+ *Pedagogical University, Cracow, Podchorążych 1, Poland.*

We performed a careful numerical analysis of the late tail behaviour of waves propagating in the Schwarzschild spacetime. Specifically the scalar monopole, the electromagnetic dipole and the gravitational axial quadrupole waves have been investigated. The obtained results agree with a falloff $1/t^{2l+3}$ for the general initial data and $1/t^{2l+4}$ for the initially static data.

I. INTRODUCTION

Waves propagating in a curved spacetime usually undergo backscatter; that leads to the emergence of two classes of effects, the so-called quasinormal modes (discovered by Vishveshvara [1]) and the tails. Price, who investigated the temporal behaviour of tails in 1972, has shown some kind of universality. The late tail behaviour of scalar, electromagnetic and gravitational waves happened to depend on the order of the multipole expansion [2]. The exposition of [2] is somewhat confusing and that forces us to say more than would normally be needed for the purpose of a paper reporting only numerical results.

Price states *If a static l-pole field is present outside the star, prior to the onset of collapse, the field will fall off as* $t^{-(2l+2)}$*. If there is no field initially outside the star, but an l-pole perturbation develops during the collapse process, it will fall off as* $t^{-(2l+3)}$ *at large time [2].* That requires a comment. Since the evolution equation (2) (see below) is linear and of the form $-\partial_t^2\Psi + L\Psi = 0$, where L is a linear time-independent operator, its solutions can be superposed. That means that if there is a static solution, then it cannot influence any evolving perturbation. Irrespective of whether there are static solutions or not, the perturbation will decay in the same way. Therefore the quoted statement cannot be taken at the face value. The natural understanding would be the following: *A static field* means that there is initially a field ($\Psi(t=0) \neq 0$), but $\partial_t\Psi = 0$ (hence data are momentarily static). *The initial absence of field* in turn means that $\Psi = 0$ but $\partial_t\Psi \neq 0$. This agrees with the standard way of posing the initial value problem in mathematical literature, and with this in mind we inspect the later papers on this subject. The notion of *initially static l-pole* has been clearly specified in two publications that appeared in late seventies; it becomes an *initially stationary multipole of order l* (that falls off like $1/t^{2l+2}$) [3]. Therein the term *initially stationary* means momentarily static as defined above, but with Ψ satisfying special asymptotic condition. On the other hand a detailed discussion in [4] shows that for *initially nonstatic,* $\partial_t\Psi \neq 0$ analytic initial data satisfying certain boundary conditions (at the event horizon of a black hole and at spatial infinity) the decay of a solution agrees with that of the Price's *initially static l-pole field.* This might suggest in turn that one can understand the "static l-pole field" as a specially prepared *general* initial wave profile. Corresponding initial data (both Ψ and $\partial_t\Psi$ are nonzero) have a noncompact support (the spatial support has infinite extension, as measured in terms of the tortoise variable r^* – see below). The work of Gundlach et al. [5] numerically confirmed the analytically derived $1/t^{2l+2}$ decay of late tails. Let us remark an internal inconsistency – the contention must be now that the fall off actually depends on the profile of initial data, in contrast to the primary expectation that the "tail" is a universal phenomenon due to the backscatter of the wave signal off the curvature of the geometry.

Leaving aside the area of *initially static fields*, let us notice that in the case of data of compact support the predictions of [2] are clear – solutions should have a falloff $t^{-(2l+3)}$. That estimate applies to solutions generated by *generic initial data* ($\Psi \neq 0$, $\partial_t\Psi \neq 0$) [4]. From a naive inspection of the formal solution $\Psi = \partial_t G * \Psi(t=0) + G * \partial_t\Psi(t=0)$ (where G is the Green function), one expects that in the case of momentarily static initial data the fall off is faster (by $1/t$) than that corresponding to general initial data. It is interesting that no numerical investigation has been performed in the case of moment of time symmetry initial data of compact support. It should be noticed also that the status of the analytic investigation is still not quite satisfactory, since it consists either of heuristic analysis [2] or rather formal investigation of the Green function formulae ([4], [6]) [8]. It is only recently that the (generic case) falloff $1/t^3$ has been rigorously proven by Dafermos and Rodnianski for the monopole mode of the real scalar field [9]. The same conclusion is being derived, in a different (spectral) method, by Machedon and Stalker [10].

The main focus of our numerical work will be on finding the falloff of tails generated by initial data of compact support in either of the aforementioned two fundamental cases. We study the evolution of the scalar monopole ($l=0$), the electromagnetic dipole ($l=1$) and the gravitational axial quadrupole ($l=2$). The obtained results reveal a falloff $1/t^{2l+3}$ for the data $\partial_t\Psi_l \neq 0, \Psi_l = 0$, in agreement with [2], and $1/t^{2l+4}$ for the initially static initial data [11]. This latter result on the behaviour of late tails generated by initial data $\partial_t\Psi_l = 0, \Psi_l \neq 0$ is

new in the numerical literature. Thus the generic initial data have the falloff $1/t^{2l+3}$, which agrees with Leaver [4], Ching et al. [6] and Poisson [7].

Our results support the view that the l-th moment of any of the waves (scalar, electromagnetic or gravitational) will decay like $1/t^{2l+3}$ for general initial data (in accordance with [6], [4] and [7]) and $1/t^{2l+4}$ for the l-th moments evolving from initially static data (in agreement with the formal analysis of [4] and [7]). These results should be of practical significance for numerical relativity. The determination of the late tail behaviour is a nontrivial but at the same time feasible numerical task that can serve as a useful test for the accuracy and stability of numerical codes.

II. DEFINITIONS AND EQUATIONS

The spacetime geometry is defined by the line element

$$ds^2 = -\eta_R dt^2 + \frac{dR^2}{\eta_R} + R^2 d\Omega^2, \tag{1}$$

where t is a time coordinate, R is the radial areal coordinate, $\eta_R = 1 - \frac{2m}{R}$ and $d\Omega^2 = d\theta^2 + \sin^2\theta d\phi^2$ is the line element on the unit sphere, $0 \leq \phi < 2\pi$ and $0 \leq \theta \leq \pi$. Throughout this paper the Newtonian constant G and the velocity of light c are put equal to 1.

The propagation of the scalar, the dipole electromagnetic and the axial (quadrupole) gravitational waves is given by

$$(-\partial_t^2 + \partial_{r^*}^2)\Psi = V\Psi. \tag{2}$$

Here $r^*(R) = R + 2m\ln\left(\frac{R}{2m} - 1\right)$ is the tortoise coordinate while the potential term reads: for the $l = 0$ mode of the scalar field

$$V(R) = 2m\frac{\eta_R}{R^3}, \tag{3}$$

for the $l = 1$ (dipole) electromagnetic mode

$$V(R) = 2\frac{\eta_R}{R^2} \tag{4}$$

and for the quadrupole axial mode of GW

$$V(R) = 6\frac{\eta_R^2}{R^2}(1 - \frac{m}{R}). \tag{5}$$

III. NUMERICAL SCHEMES

We will choose following classes of initial data:

i) $\Psi(R, t = 0) = \sin^4\left(\pi\frac{r^* - r^*(a)}{4m}\right)$ and $\partial_t\Psi|_{t=0} = -\partial_{r^*}\Psi_{t=0}$ for $r^* \in (r^*(a) = r^*(3m), r^*(a) + 4m)$, and $\Psi(r, 0) = \partial_t\Psi = 0$ for $r^* < r^*(a)$ or $r^* > r^*(a) + 4m$. The expected asymptotic tail falloff should be the same as for generic initial data.

ii) Symmetric initial data with $\Psi(R, t = 0) = \sin^4\left(\pi\frac{r^* - r^*(a)}{4m}\right)$ for $r^* \in (r^*(a) = r^*(3m), r^*(a) + 4m)$ and $\Psi(r, 0) = 0$ for $r^* < r^*(a)$ or $r^* > r^*(a) + 4m$, and $\partial_t\Psi_{t=0} = 0$ everywhere. It is shown below that the corresponding tail decays faster than that of i).

iii) $\partial_t\Psi = \sin^4\left(\pi\frac{r^* - r^*(a)}{4m}\right)$ for $r^* < r^*(a) = r^*(3m)$ or $r^* > r^*(a) + 4m$ and $\partial_t\Psi(r, 0) = 0$ for $r^* < r^*(a)$ or $r^* > r^*(a) + 4m$, while $\Psi|_{t=0} = 0$ everywhere; the tail behaviour happens to be like in i).

One finds convenient to split the wave equation (2), into the pair of first order differential equations

$$(\partial_t + \partial_{r^*})\Psi = \Phi \tag{6}$$

$$(\partial_t - \partial_{r^*})\Phi = -V(r^*)\Psi. \tag{7}$$

We use the following mesh scheme (see Fig. 1)

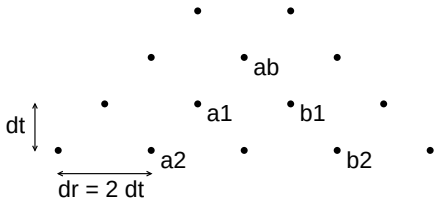

FIG. 1. This figure shows the mesh used in the numerical computations. In the one-step scheme the functions Φ_{ab}, Ψ_{ab} are computed from Eqs (9 – 11) using values at points $a1$ and $b1$. The second algorithm needs values at four points $a1, a2, b1$ and $b2$ in order to obtain Φ_{ab}, Ψ_{ab} from Eqs (14).

and two differencing schemes: the one-step implicit alghoritm and the multistep Adams-like algorithm. In the first approach we approximate the equations (7) by

$$\Psi_{ab} - \Psi_{a1} = (\Phi_{ab} + \Phi_{a1})\frac{dt}{2} \tag{8}$$

$$\Phi_{ab} - \Phi_{b1} = -(V_{ab}\Psi_{ab} + V_{b1}\Psi_{b1})\frac{dt}{2}. \tag{9}$$

In the next step these equations are solved for Ψ_{ab}, Φ_{ab},

$$\Psi_{ab} = \Psi_{ab}(\Psi_{a1}, \Psi_{b1}, \Phi_{a1}, \Phi_{b1}) \tag{10}$$

$$\Phi_{ab} = \Phi_{ab}(\Psi_{a1}, \Psi_{b1}, \Phi_{a1}, \Phi_{b1}). \tag{11}$$

The second alghoritm is based on the Adams-Moulton corrector formula for ordinary differential equations [12]

$$y_{n+1} = y_n + \frac{dt}{12}(5y'_{n+1} + 8y'_n - y'_{n-1}) + O(dt^4) \tag{12}$$

Applying this formula to each of the equations (7) we get approximatelly

$$\Psi_{ab} = \Psi_{a1} + \frac{dt}{12}(5\Phi_{ab} + 8\Phi_{a1} - \Phi_{a2}) \tag{13}$$

and

$$\Phi_{ab} = \Phi_{b1} - \frac{dt}{12}(5V_{ab}\Psi_{ab} + 8V_{b1}\Psi_{b1} - V_{b2}\Psi_{b2}) \tag{14}$$

Again this linear set of equations can be solved for Ψ_{ab}, Φ_{ab}

$$\begin{aligned}\Psi_{ab} &= \Psi_{ab}(\Psi_{a1}, \Psi_{b1}, \Psi_{a2}, \Psi_{b2}, \Phi_{a1}, \Phi_{b1}, \Phi_{a2}, \Phi_{b2}) \\ \Phi_{ab} &= \Phi_{ab}(\Psi_{a1}, \Psi_{b1}, \Psi_{a2}, \Psi_{b2}, \Phi_{a1}, \Phi_{b1}, \Phi_{a2}, \Phi_{b2}).\end{aligned} \tag{15}$$

Let us stress that these two alghoritms give almost the same results, hinting at the numerical stability of our methods.

IV. NUMERICAL RESULTS

We expect the field $\Psi_l(r^*, t)$ to behave (for a fixed r^*) like

$$\lim_{t\to\infty} \Psi(r^*, t) = Ct^{-\alpha} \tag{16}$$

Our goal is to get a value of α with a reasonable accuracy. Therefore we calculate the function

$$f(t) = -\frac{d\log(\Psi_l(r^*, t))}{d\log(t)} = -t\frac{d\log(\Psi_l(r^*, t))}{dt} \tag{17}$$

which asymptotically should be equal to α.

In the first instance we analysed the case with waves, which belongs to the class i) of Sec. 3, and for the initial data of class iii) of the preceding section. The results are presented in Figs. 2 – 4 which show the temporal behaviour of the funtion $f(t)$ as seen at $r^* = r^*(3m)+4m$. In all figures (2 – 7) below the time is put on the x-axis, which is scaled in units of m.

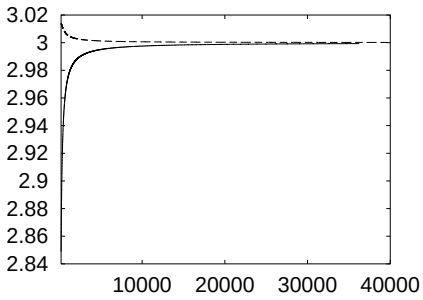

FIG. 2. The solid (general initial data) and broken line (data with $\phi = 0$), the behaviour of $f(t)$ for the scalar waves.

The numerical time ranged from 5000 m (for the gravitational and electromagnetic waves) up to 40000 m (for the scalar waves). It turned out that the precise shape of this function, without numerical noise, can be calculated using numbers with 64 significant digits (gravitational and electromagnetic cases) and the ordinary double precision numbers (scalar case). In order to achieve this aim we have used the freely distributable "qd" (quad precision) and "arprec" (arbitrary precision) numerical libraries [13].

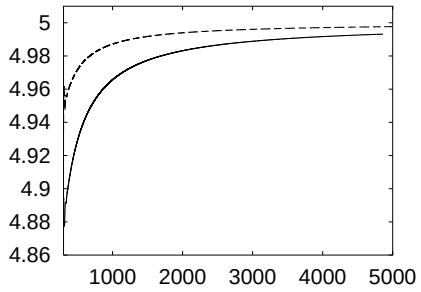

FIG. 3. The solid (general initial data) and broken line (data with $\phi = 0$), the behaviour of $f(t)$ for the selectromagnetic waves.

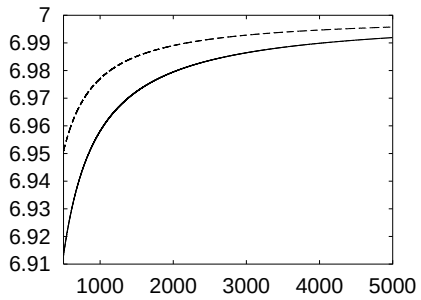

FIG. 4. The solid (general initial data) and broken line (data with $\phi = 0$), the behaviour of $f(t)$ for the gravitational waves.

The high accuracy calculations are time consuming and therefore the achieved calculational time for the scalar case exceeds by a factor of 8 the evolution time for the remaining cases. The numerically achieved values of the exponent , for the general initial data i), range from 2.999 for the scalar field, through 4.99 for the electromagnetic field up to 6.99 for the gravitational waves (figures 2 – 4, solid line). Both sets of exponents is in a good agreement with 3, 5 and 7, respectively, obtained by Ching et al. [6]. Similar results (broken line Fig. 3) have been obtained for the initial data of class iii) of the preceding section, in agreement with [2].

The momentarily static initial data (class ii) from Sec. 3) produced profiles $f(t)$ shown in Figs. 5 – 7. In this case the numerical exponents have been determined at $r^*(b) = r^*(3m) + 4m$ and also at another obervation

point, $r^* = 100m + r^*(b)$. In the first case we obtained 4, 6 and 8 (up to the fourth digit number) while in the latter case we arrived at 3.99, 5.88 and 7.84, for the scalar, electromagnetic and gravitational waves, respectively. These exponents seem to be stabilize at 4, 6 and 8 for the scalar, electromagnetic and gravitational fields, respectively; notice that the results detected at $r^* = r^*(3m) + 4m$ converge quicker to the prospective limiting value than those taken at the point located farther. The asymptotic tail regime is evidently achieved quicker at a region closer to the horizon, which is a new feature, unknown in the existing literature. But in both detection points, the asymptotic values of α are similar and very close in the case of the scalar waves, see Fig. 5. The calculation of these exponents constitutes the main result of this paper.

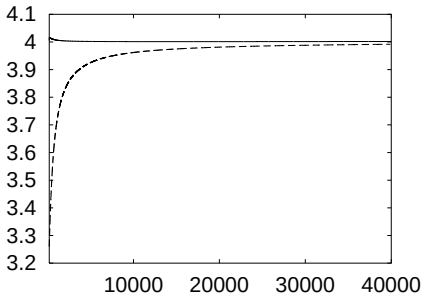

FIG. 5. Time-symmetric initial data. The solid and broken lines show the behaviour of $f(t)$ for scalar waves, as seen at the observation points $r^*(b) = r^*(3m) + 4m$ and $r^* = r^*(b) + 100m$, respectively.

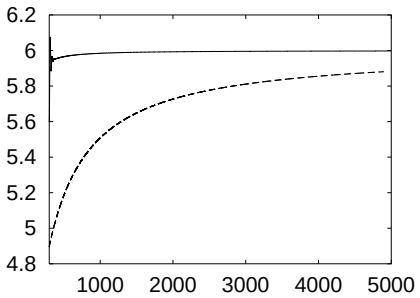

FIG. 6. Time-symmetric initial data. The solid and broken lines show the behaviour of $f(t)$ for electromagnetic waves, as seen at the observation points $r^*(b) = r^*(3m) + 4m$ and $r^* = r^*(b) + 100m$, respectively.

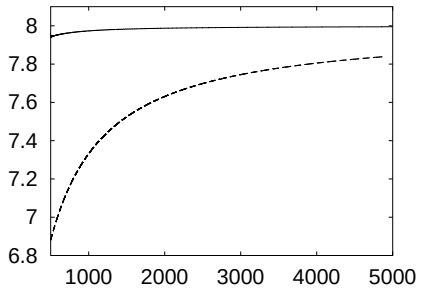

FIG. 7. Time-symmetric initial data. The solid and broken lines show the behaviour of $f(t)$ for gravitational waves, as seen at the observation points $r^*(b) = r^*(3m) + 4m$ and $r^* = r^*(b) + 100m$, respectively.

Acknowledgments. This work has been supported in part by the KBN grant 2 PO3B 006 23. One of us (EM) acknowledges a discussion with Eric Poisson.

[1] C. V. Vishveshwara, *Nature* **227**, 936(1970).
[2] R. Price, *Phys. Rev.* **D5**, 2419(1972).
[3] C. T. Cunningham, R. Price and V. Moncrief, *Astr. J.* **224**, 643(1978); *ibid*, **230**, 870(1979).
[4] E. W. Leaver, *Phys. Rev.* **D34**, 384(1986).
[5] C. Gundlach, R. Price and J. Pullin, *Phys. Rev.* **D49** 883(1994); *ibid*, 890(1994).
[6] E. S. C. Ching P.T. Leung, W.M. Suen, K. Young, *Phys. Rev.* **D52**, 2118(1995).
[7] E. Poisson, *Phys.Rev.* **D66**, 044008(2002).
[8] J. Bicak, *Gen. Rel. Grav.* **3**, 331(1972); *ibid*, **12**, 195(1980); S. Hod, *Phys. Rev.* **D58**, (1998) 024019.
[9] M. Dafermos and I. Rodnianski, *A proof of Price's law for the collapse of a self-gravitating scalar field* gr-qc/0309115.
[10] John Stalker, private communication.
[11] From now on we do not make distinction between data that are *initially static*, *momentarily static* or *moment of time symmetry initially.*
[12] W. H. Press, S. A. Teukolsky, W. T. Vetterling and B. P. Flannery, Numerical Recipes in C, Oxford Press.
[13] Quad: Y. Hida, X. S. Li and D. H. Bailey; arprec: Y. Hida X. S. Li. H. Bailey and B. Thompson. Available at http:// users.bigpond.net.au/amiller.